Supporting Information for Inefficient Consumption of Natural Gas Drives Methane Emissions from a Megacity

Yuwei Zhao[1,2], Andrew Hallward-Driemeier[1,2], Luke D. Schiferl[2], Trey Maddaleno[3], Michael P. Vermeuel[4], Dylan B. Millet[3], Delphine Farmer[5], and Róisín Commane[1,2]

[1]Department of Earth and Environmental Sciences, Columbia University, New York, NY 10027, USA
[2]Lamont-Doherty Earth Observatory, Columbia University, Palisades, NY 10964, USA
[3]Department of Soil, Water, and Climate, University of Minnesota, St. Paul, MN 55108, USA
[4]Department of Earth, Atmospheric, and Planetary Sciences, Purdue University, West Lafayette, IN, 47907, USA
[5]Department of Chemistry, Colorado State University, Fort Collins, CO 80523, USA

Correspondence: Yuwei Zhao (yz4343@columbia.edu)

Section S1 to S13

Figures S1 to S13

Tables: S1 to S3

Section 1: Detailed Instrument Calibration and Uncertainties for Tower-based Measurements

The Columbia Aerodyne SuperDUAL spectrometer was deployed to measure 1 Hz methane (CH_4), ethane (C_2H_6), carbon monoxide (CO), carbon dioxide (CO_2), nitrous oxide (N_2O) mole fractions, and water vapor. The SuperDUAL is a cavity-enhanced infrared direct absorption spectrometer equipped with a double-laser systemCommane et al. (2023).

A dry compressed air calibration tank was sampled hourly to account for internal instrument variations. Additionally, high-span (HS) calibration and low-span (LS) tanks were sampled once every day calibrate all measurements to the NOAA GM-L/WMO scale: methane (WMO X2004A), CO2 (WMOX2019), CO(WMOX2014A); and an internal CCL scale for ethane (C_2H_6-2012) and N2O (NOAA-2006A). SuperDUAL measurements are sensitive to humidity changes. To address this, humidity corrections based on the method described by Commane et al., (2023) were applied to CH_4, C_2H_6, CO, CO_2, and N_2O before performing LS and HS calibrations Commane et al. (2023). On August 8^{th}, 2023 calibration runs of the compressed air tank from the multi-trace gas measurements exhibited abnormal variance, likely due to excessive temperatures in the shed. Data from these clean-air intrusion periods in June and July, and abnormal measurements from the multi-trace gas measurements on August 8^{th}, 2023 were excluded.

Measurement variations due to instrument changes were evaluated to be negligible compared to the variability observed in ambient trace gas concentrations. For methane (CH_4), standard deviations from tank calibration were 0.13 ppb (relative standard deviation [RSD] 0.006%) with the old computer and 0.18 ppb (0.008%) with the new computer after July 21^{st}. Ethane (C_2H_6) exhibited greater variability than methane, with average standard deviations of 0.03 ppb (0.61%) before the computer failure and 0.05 ppb (1.58%) after switching to the new computer. Carbon monoxide (CO) variations were 0.5 ppb (0.11%) with the old computer and 0.6 ppb (0.13%) with the new one. N_2O variations were 0.1 ppb (0.019%) with the old computer and 0.03 ppb (0.008%) with the new computer.

The computer of the SuperDUAL failed on July 6th, 2023, likely due to the excessively hot temperatures in the measurement shed, which often exceeded 35°C. The new computer setup was operational from July 21^{st}, 2023.

Dry mole fractions of methane at LDEO were measured on a Picarro G2301 and calibrated to the WMO scale for methane (WMO X2004A). These measurements are corrected for water vapor effects to estimate the dry mole fraction. Measurement uncertainties are smaller than the variability in methane mixing ratios measured at this site, with the typical hourly standard deviation of methane mixing ratios around 10 ppb. Stockholm, Camden, and Waterford are part of the NIST network and calibrated in the same manner as the NIST-MNY site, and the uncertainty archived at an hourly time resolutionKarion et al. (2023); Verhulst et al. (2017); Welp et al. (2013); Karion et al. (2020).

Section 2: Wildfire Events and Non-local Air Observations

Smoke from Quebec wildfires severely impacted air quality in NYCMA during the summer 2023, with elevated CO dry mole fractions observed at the Mineola tower from June 5^{th} to 9^{th} and again from June 28^{th} to July 3^{rd}, 2023 (Figure S1). We exclude wildfire events from city-scale methane emission source attribution analysis.

A regional methane depletion was observed at the northern and eastern sites (MNY, HCT, and LDEO) from June 16^{th} to June 25^{th}, 2023. At the Mineola tower, methane, CO, and ethane dry mole fractions dropped below what is typically considered a background for this location, with dry mole fractions reaching 1936 ppb for methane, 69 ppb for CO, and below 0.5 ppb for ethane (Figure S1). Methane depletion was also observed at Mineola from July 9^{th} to 11^{st}, July 15 th to 17 th, and August 7^{th} to 9^{th} 2023 from NIST-MNY observations when campaign-based measurements were not available. These observations suggest an intrusion of non-local clean marine air masses, and we have excluded these times from the campaign-based methane source attribution analysis.

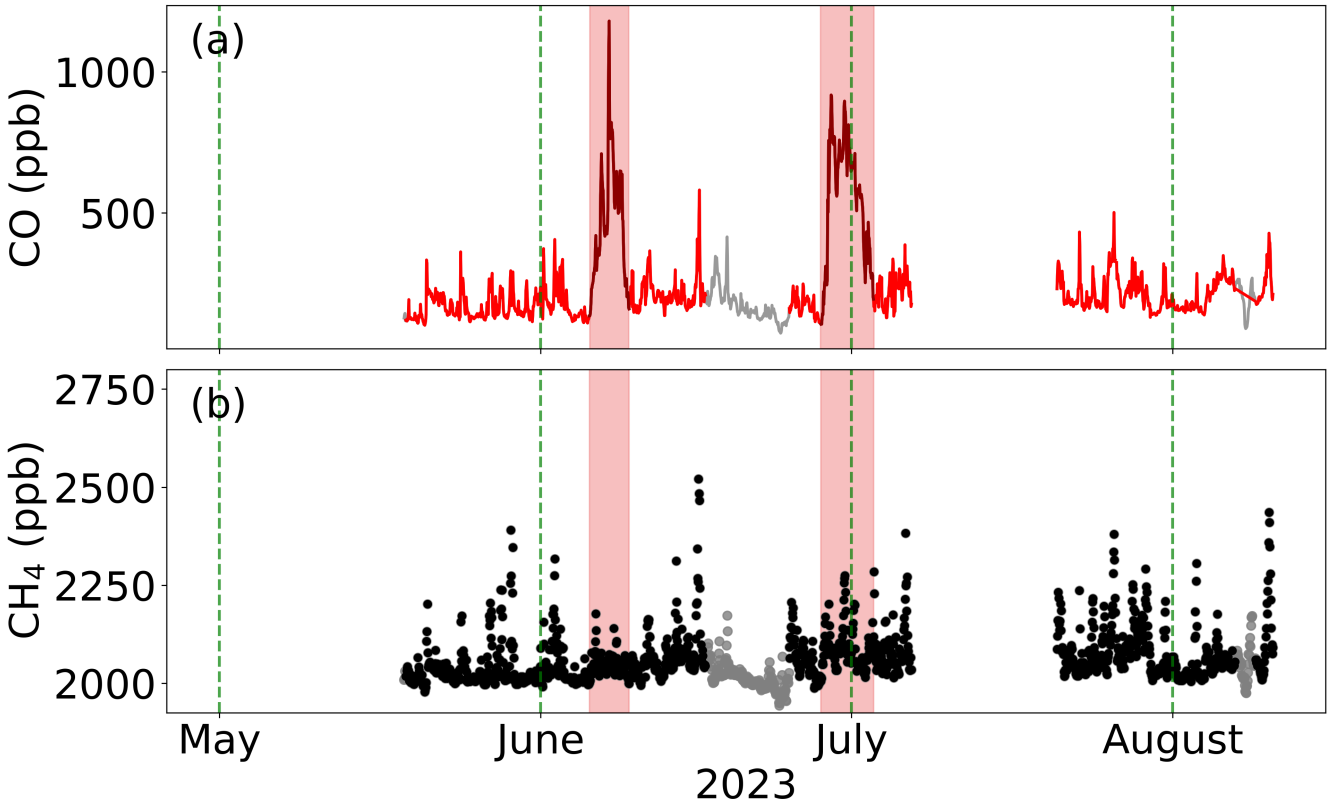

Figure S1. (a) Time series of summer campaign-based hourly trace gas dry mole fractions sampled from the Mineola Tower at 60 m (FROG-NY Multi-trace gas measurements) of (a) CO (red line) and (b) methane (black circles) for May 19^{th} to August 10^{th}, 2023. Non-local air observations (grey line for CO and grey circles for methane) and periods of elevated CO associated with smoke transported from Canadian wildfires in Quebec (red shading; June 5th to 8th and June 28th to July 3^{rd}) have been excluded from the source attribution analysis.

Section 3: Street-level Observations

NYAAQ mobile lab was equipped with Aeris MIRA Ultra analyzers, with the CH_4/C_2H_6 analyzer described in detail by Commane et al. (2023) Commane et al. (2023). The trace gas inlet and an AirMar 220WX-RH Weather Station were mounted at the center of the vehicle's roof, approximately 2 meters above the ground. The MIRA Ultra analyzers were powered by a lithium battery connected to an inverter, and all instruments were securely grounded within the vehicle's trunk on a wooden board. To account for instrument delay, breath tests were performed to determine the tubing lag time between the inlet and the analyzer cell, which was approximately 7 seconds. Typical driving speeds of 6 to 12 m/s, combined with an analyzer cell flushing time of $\tilde{9}.5$ seconds, provided a spatial resolution of about 60 to 100 meters for trace gas measurements.

During the mobile sampling drive (Figure S2), we observed two pipeline leaks with strong correlations between methane and ethane, with no correlations between methane and CO despite nearby sources such as traffic. We did not see consistent street-level co-peaks of CO and natural gas (methane and ethane).

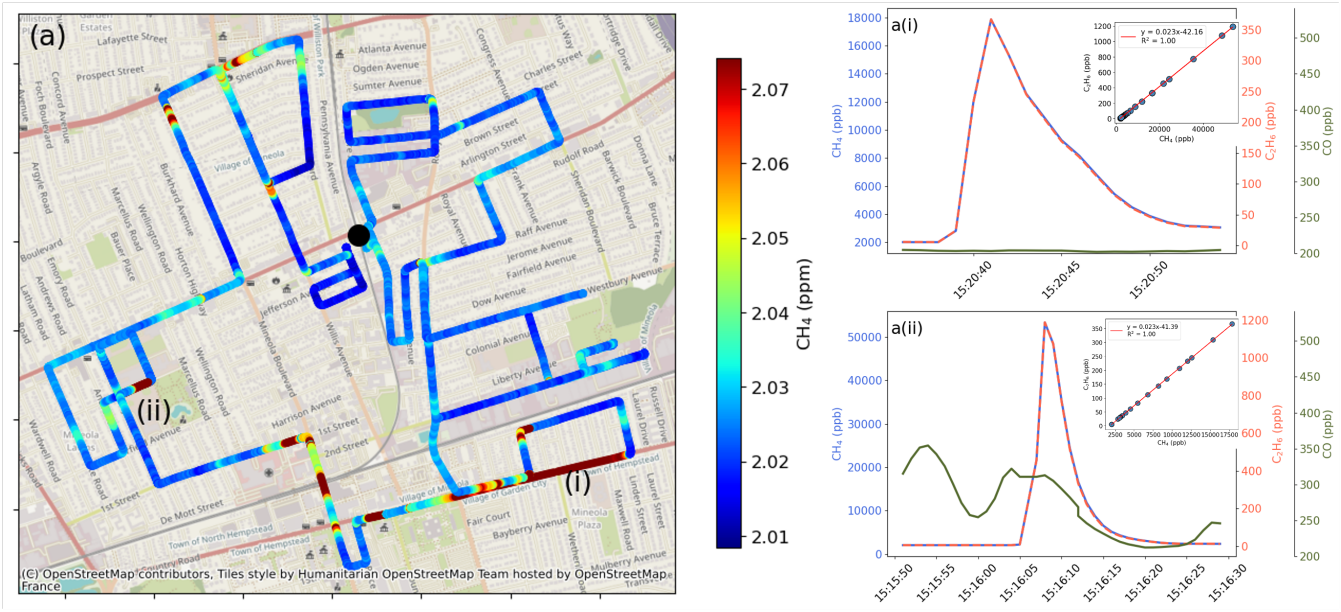

Figure S2. Maps of mobile sampling colored by (a) CH_4 and (b) C_2H_6 mole fractions illustrate two natural gas pipeline leaks with a C_2H_6:CH_4 ratio of 2.3%, as shown in plots a(i) and a(ii), CO is shown in a(i) and a(ii) as green lines.

Section 4: Background Calculation

Table S1. Remote sites used to calculate background methane mole fractions

	Stockholm	Hamden	Lamont-Doherty Earth Observatory
Site ID	SNJ	HCT	LDEO
Latitude (°N)	41.14356	41.43371	41.00218
Longitude (°W)	74.5387	72.9452	73.9097
Altitude (m agl)	53	115	18

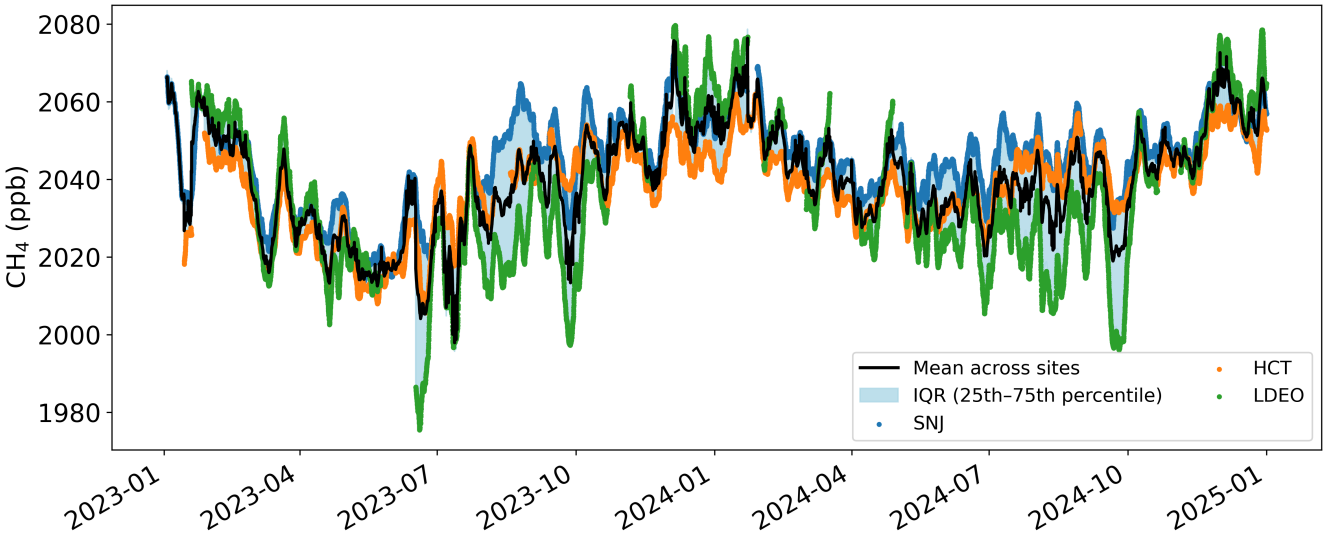

Figure S3. Time series of methane background at HCT (orange), LDEO (green), and SNJ (blue). The black line shows the mean background, and the blue shading indicates the 25^{th} to 75^{th} percentile background range derived from bootstrapped hourly methane dry mole fractions across the three rural sites, using a 240-hour running window.

Section 5: Source Attributions

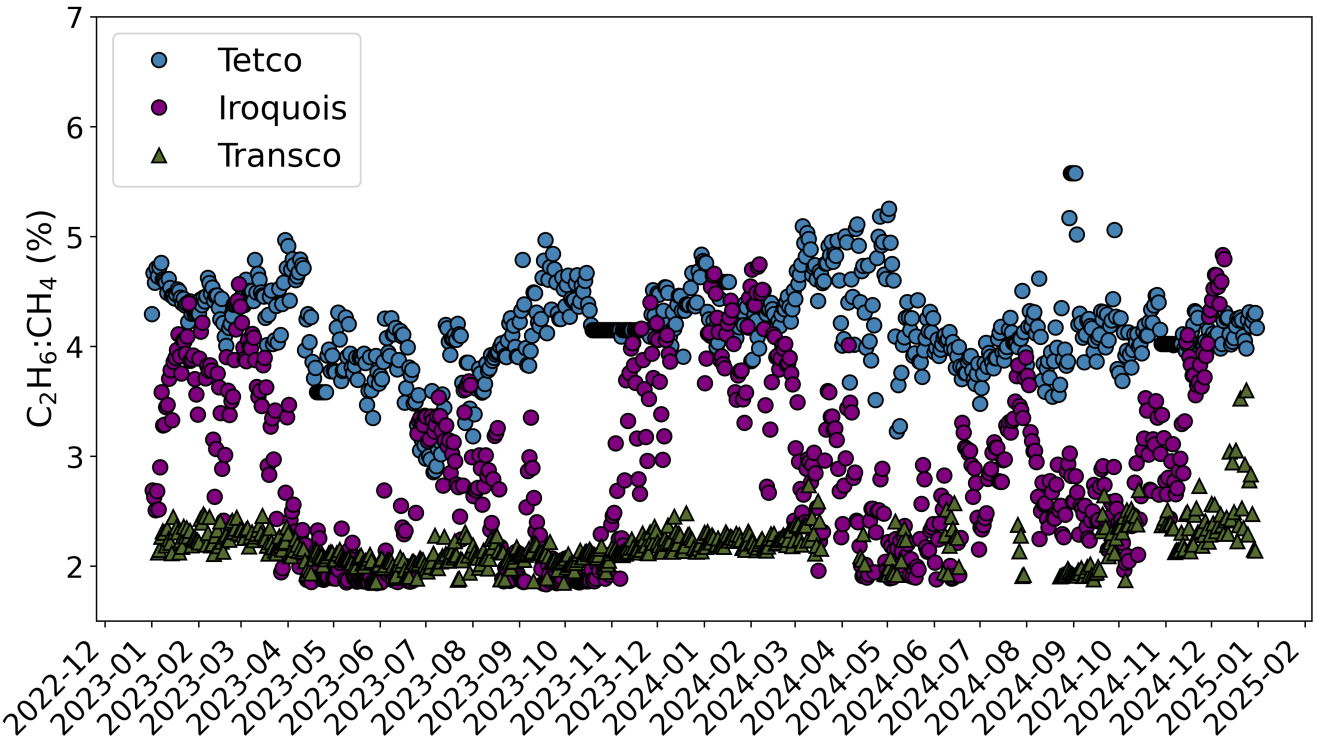

Figure S4. Timeseries of reported daily ethane-to-methane ratio (%) from Tetco (blue) and Transco (green), and Iroquois (purple) from January 2023 to December 2024.

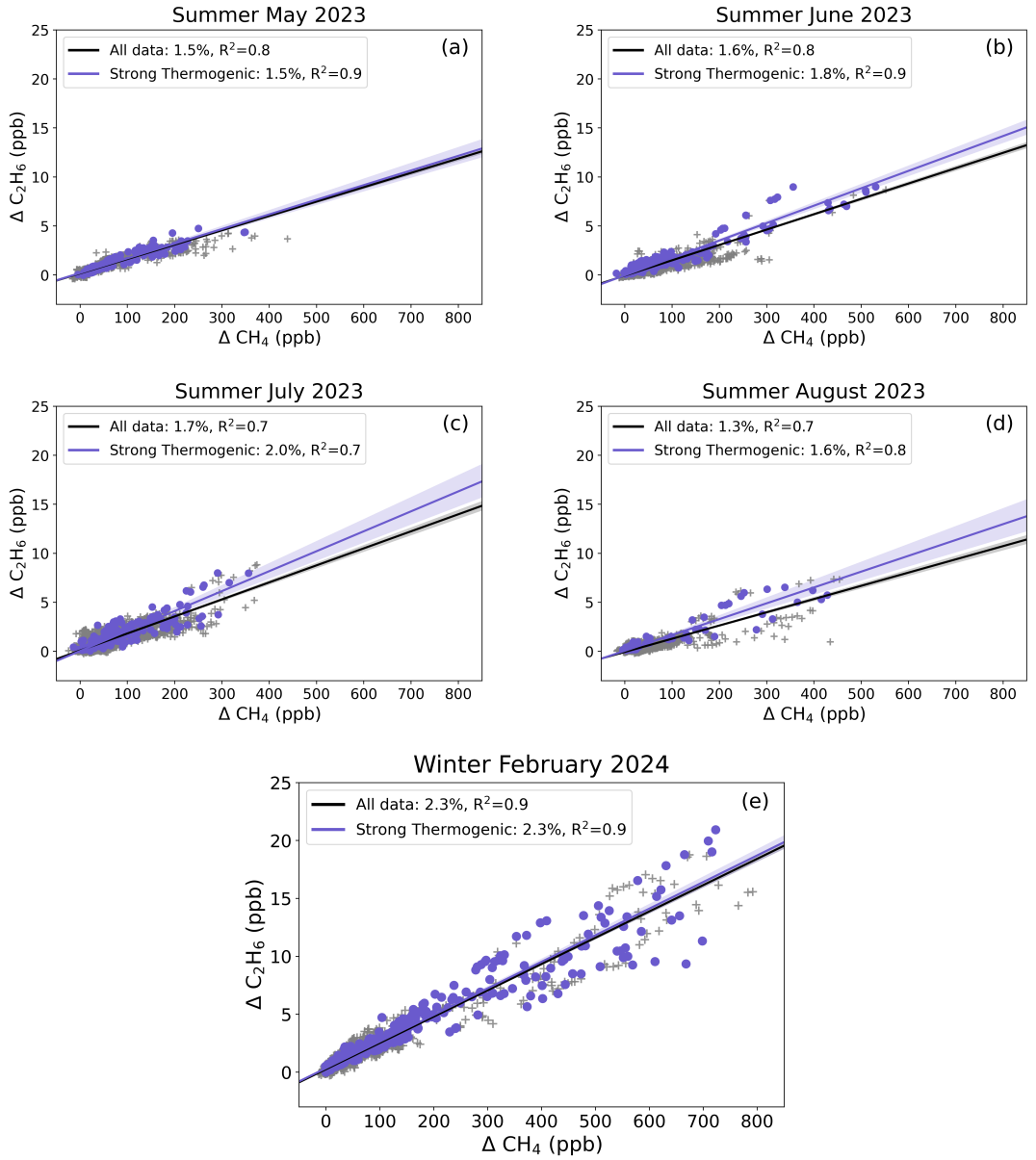

Figure S5. Scatter plot of 5-minute average ΔC_2H_6 vs ΔCH_4 for (a) May, (b) June, (c) July, (d) August, 2023, and (e) February, 2024. In each plot, all observed 5-minute data are plotted as gray crosses and the RMA linear regression is represented as black lines with 95% CI shown in gray shading. Thermogenic plumes with $R^2_{\Delta C_2H_6:\Delta CH_4} \geq 0.95$ are shown in purple circles and linear regression of thermogenic ΔC_2H_6:ΔCH_4 are shown in purple lines, with purple shading representing 95% CI.

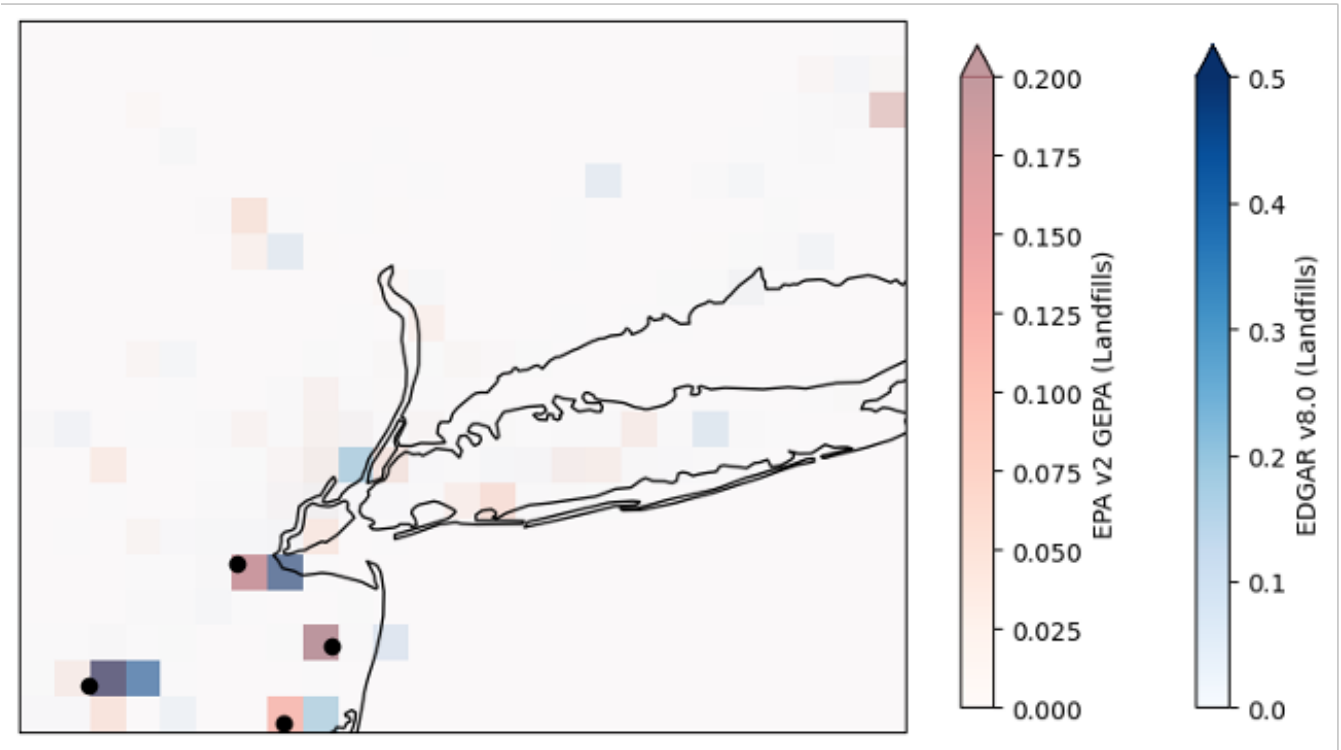

Figure S6. Map of the landfill sector in NYCMA as represented in the gridded EPA v2 inventory for 2018 (red) and in the EDGAR v8.0 inventory for 2022 (blue). The locations of large active landfills (black dots) are not accurately represented in EDGAR, with many sources shifted to grid boxes east of their actual locations.

Table S2. Methane inventories included in this study

Inventory	Year	Temporal Resolution	Spatial Resolution	Coverage
GEPA	2018	Monthly	$0.1 \times 0.1°$	U.S.A.
EPA Extension	2018	Monthly	$0.1 \times 0.1°$	U.S.A.
EDGAR v6.0	2018	Monthly	$0.1 \times 0.1°$	Global
EDGAR v8.0	2022	Monthly	$0.1 \times 0.1°$	Global
Pitt et al. (2024)	2019	Annual	$0.02 \times 0.02°$	NY-Newark

Section 7: Monthly Footprints at Mineola Tower

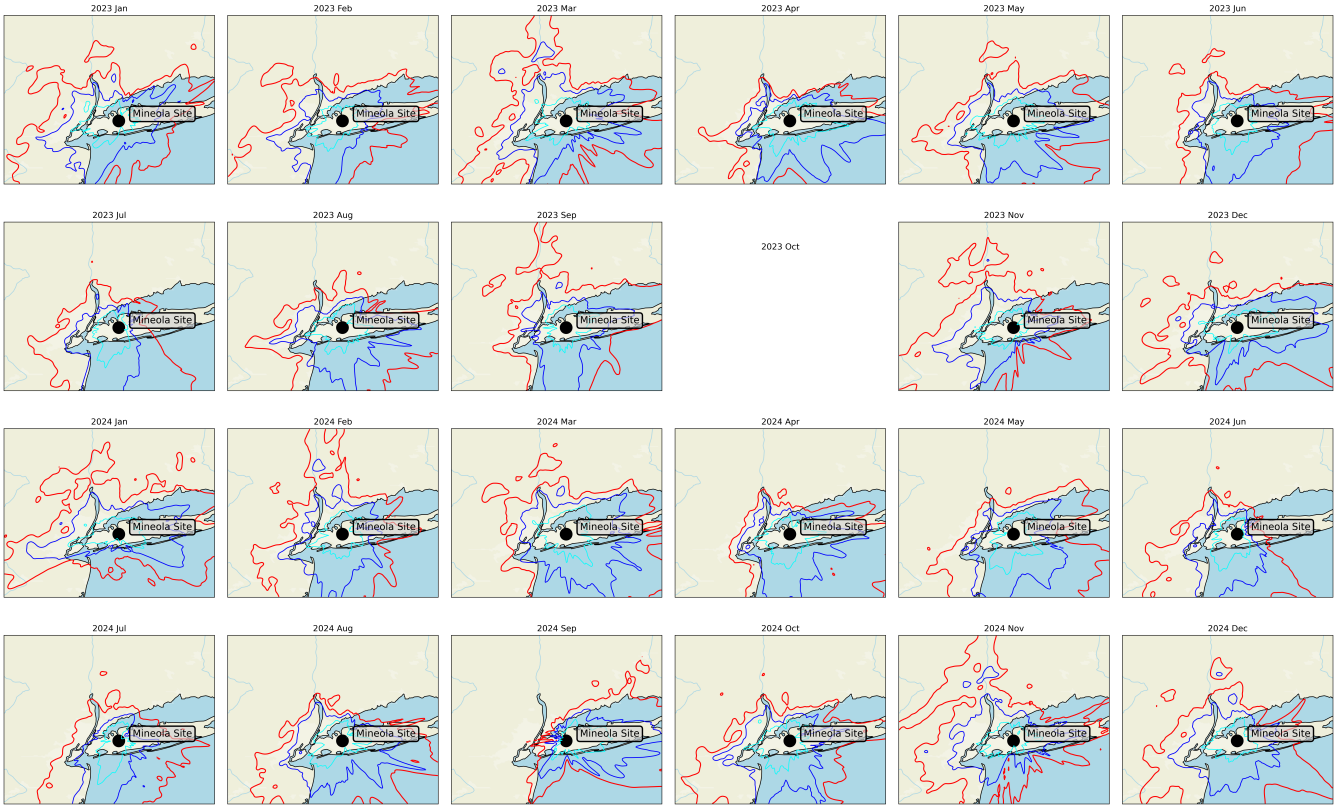

Figure S7. Map of monthly footprint contour at the Mineola Tower at 62 m AGL over the NYCMA domain. The solid contours indicate the 50% (cyan), 75% (blue), and 90% (red) surface influence footprints.

Section S8: Atmospheric Transport Model

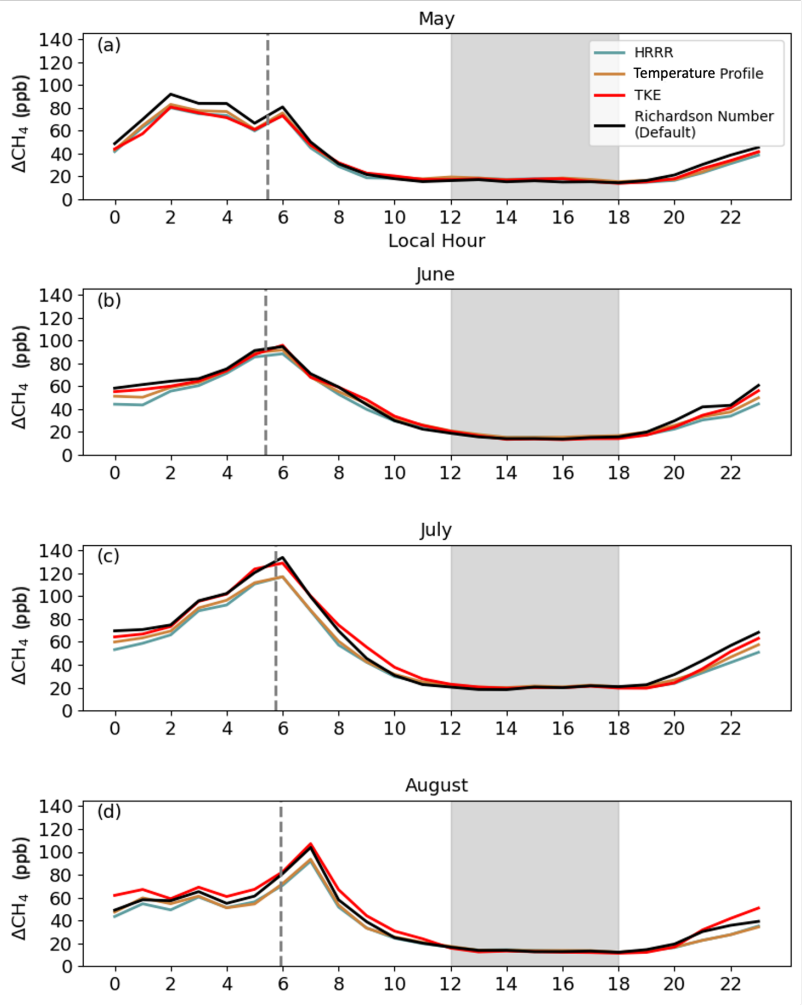

Figure S8. Diel cycles of simulated CH_4 enhancements calculated using the HRRR-STILT atmospheric transport model for (a) May, (b) June, (c) July, and (d) August. Sensitivity analysis on the mixed layer height was performed using four methods: Richardson number method (black), HRRR-derived mixed layer height (blue), temperature profile method (orange), and turbulence kinetic energy method (red). The smallest differences between methods were observed in the afternoon (12:00–18:00 EDT, grey shading). Sunrise times are indicating as grey vertical dash-lines.

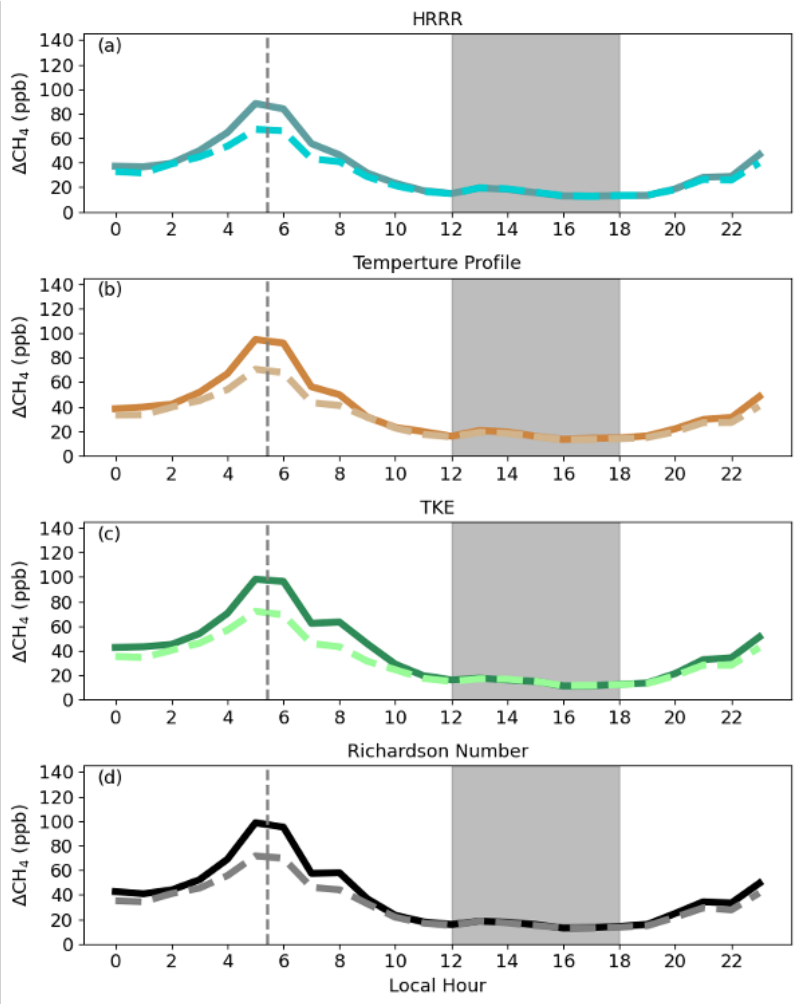

Figure S9. Diel cycles of simulated CH_4 enhancements calculated using two configurations in the HRRR-STILT atmospheric transport model from June 17 to June 25, 2023: a minimum mixed layer height of 250 m (solid line) versus 150 m (dashed line). Simulations are shown for (a) embedded HRRR, (b) temperature profile method (orange), (c) turbulence kinetic energy method (green), and (d) default Richardson number method. The smallest differences between methods were observed in the afternoon (12:00–18:00 EDT, grey shading). For subsequent simulations, the default minimum mixed layer height of 150 m was applied. Sunrise times are indicates as grey vertical dash-lines.

Section S9: Diel cycle of Observed and Simulated ΔCH_4

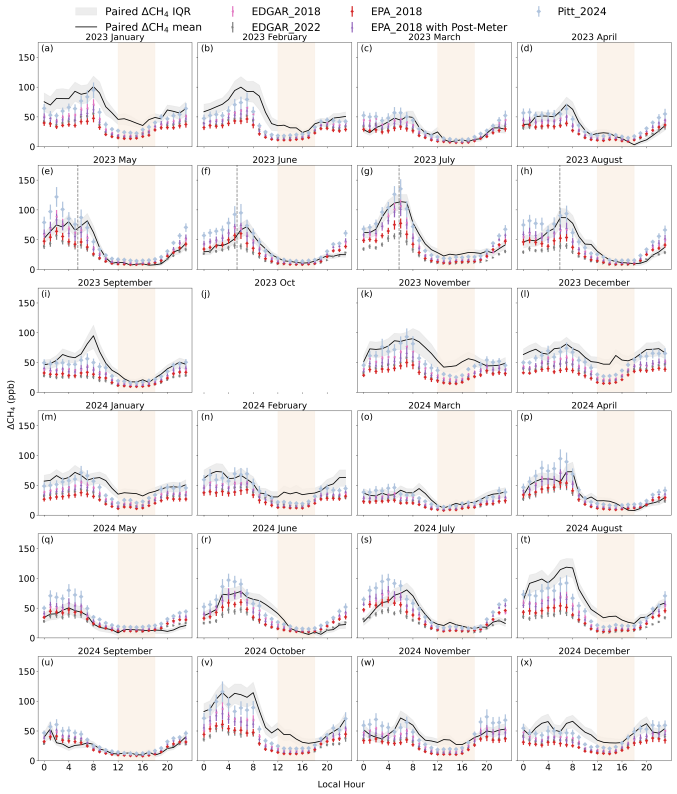

Figure S10. Diel cycle of NIST-MNY observed and simulated ΔCH_4 for the Mineola Tower from 2023 to 2024. Observed ΔCH_4 is shown as black lines, and the 50% CI is represented as grey shading. The monthly mean ΔCH_4 diel cycle was calculated using a bootstrap resampling method (n = 1000) on hourly ΔCH_4 over the averaging period. The confidence interval accounts for uncertainties arising from the background calculation and the variability of the observed methane dry mole fractions within that month. Simulated ΔCH_4 were derived from multiple inventories convolved with the surface influence footprints: Pitt inventory (blue, with 50% CI error bar), GEPA 2018 (red, with 50% CI red error bar), Extended GEPA 2018 (purple, with 50% CI red error bar), EDGAR 2018 (pink, with 50% CI red error bar), and GEPA 2022 (grey, with 50% CI red error bar). Note that none of the inventories include diel cycles in emissions and all the variability in the simulated ΔCH_4 is driven by the atmospheric transport model.

Section S10: Comparison of ASRC urban core and Mineola Suburban CH_4 Observations

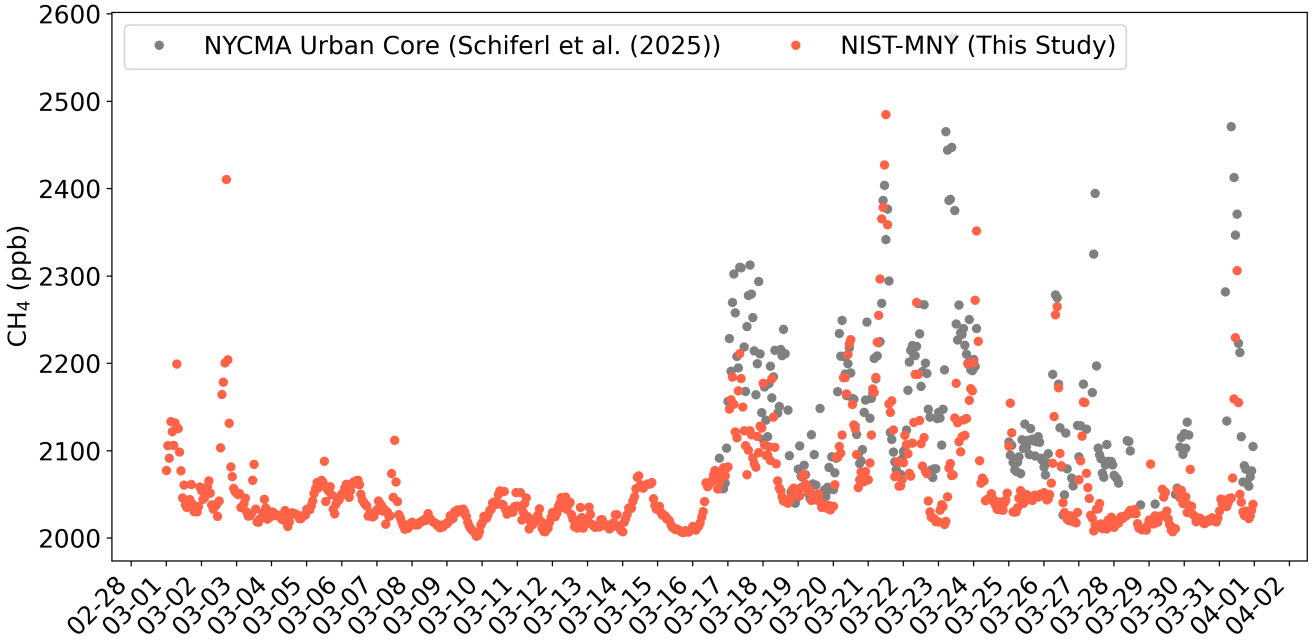

Figure S11. Hourly methane timeseries measured at ASRC located at NYCMA urban core (gray) and NIST-MNY (red) in March 2023.

Section S11: Observation Informed Methane Emission Rates

Table S3. Monthly observation-informed methane emission rates from NYCMA with 95% confidence intervals (kg s^{-1})

Month	2023	2024
January	15.3 ± 3.6	15.0 ± 4.2
February	14.4 ± 4.4	15.6 ± 4.8
March	9.3 ± 4.6	10.6 ± 4.6
April	9.0 ± 4.7	9.9 ± 4.1
May	6.0 ± 3.4	6.5 ± 5.1
June	9.1 ± 7.6	9.2 ± 6.0
July	13.2 ± 6.2	11.1 ± 7.6
August	10.1 ± 12.1	16.8 ± 10.0
September	11.7 ± 8.2	7.9 ± 10.2
October		17.5 ± 4.8
November	15.9 ± 4.4	13.5 ± 3.6
December	14.9 ± 4.0	12.4 ± 4.1

Section S12: Thermogenic Methane Incomplete Combustion Signal Histograms

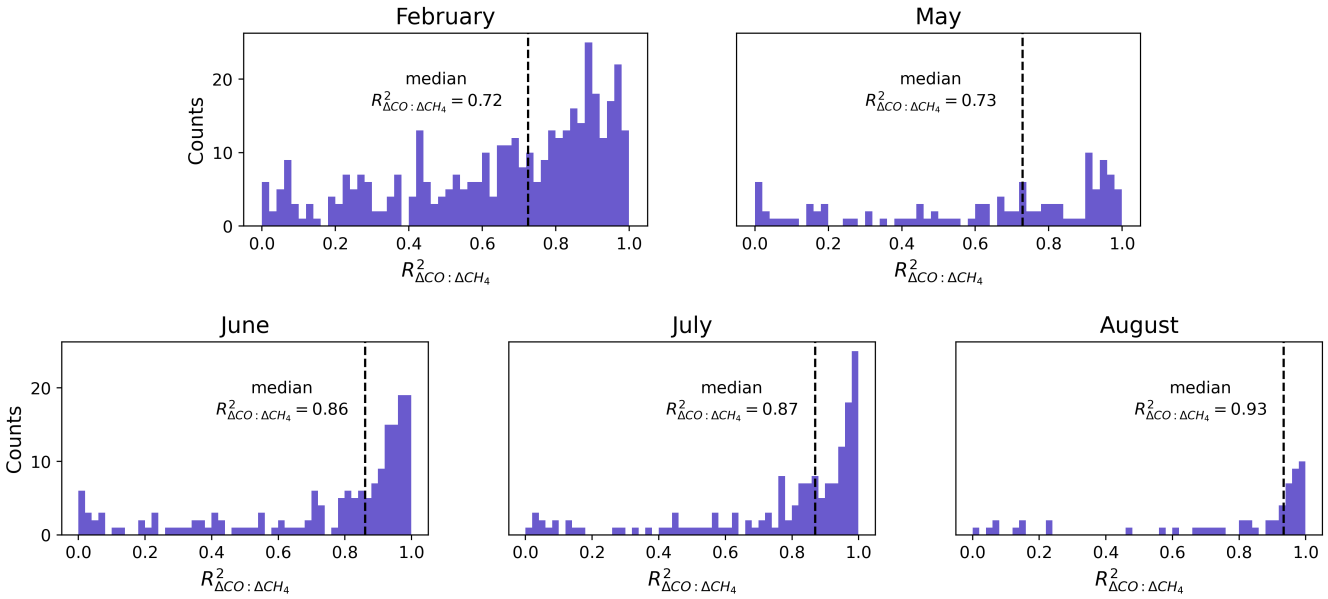

Figure S12. Histogram of correlations between 1 Hz ΔCO and ΔCH_4 within each 5-minute interval for thermogenic observations ($R^2_{\Delta C_2H_6:\Delta CH_4} \geq 0.95$)

Section S13: Natural gas Loss Rate

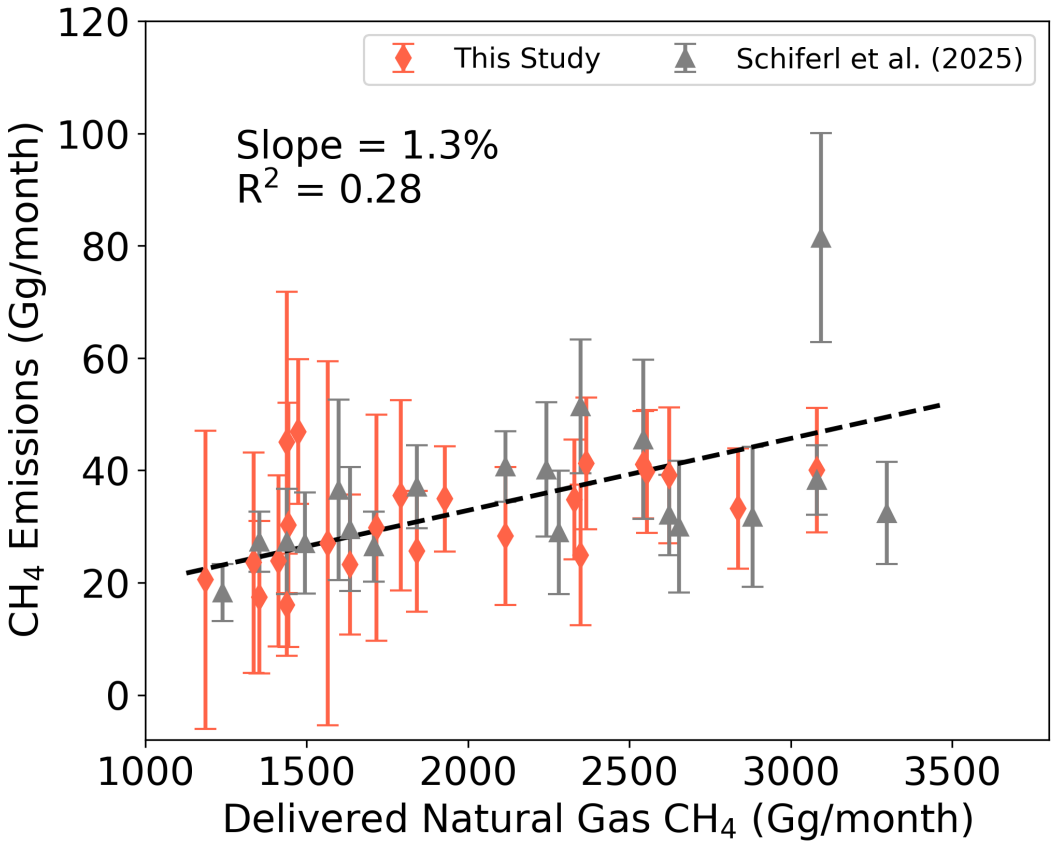

Figure S13. Observation-based total methane emissions (this study in red and Schiferl et al. (2025) in gray) compared to natural gas methane delivered to NYC and northeast NJ.

References

Commane, R., Hallward-Driemeier, A., and Murray, L. T.: Intercomparison of commercial analyzers for atmospheric ethane and methane observations, Atmospheric Measurement Techniques, 16, 1431–1441, https://doi.org/10.5194/amt-16-1431-2023, 2023.

Karion, A., Callahan, W., Stock, M., Prinzivalli, S., Verhulst, K. R., Kim, J., Salameh, P. K., Lopez-Coto, I., and Whetstone, J.: Greenhouse gas observations from the Northeast Corridor tower network, Earth System Science Data, 12, 699–717, https://doi.org/10.5194/essd-12-699-2020, 2020.

Karion, A., DiGangi, E., Prinzivalli, S., Draper, C., Baldelli, S., Fain, C., Biggs, B., Stock, M., Michalak, B., Salameh, P., Kim, J., Callahan, W., and Whetstone, J.: Observations of carbon dioxide (CO2), methane (CH4), and carbon monoxide (CO) mole fractions from the NIST Northeast Corridor urban testbed, https://doi.org/10.18434/MDS2-3012, 2023.

Verhulst, K. R., Karion, A., Kim, J., Salameh, P. K., Keeling, R. F., Newman, S., Miller, J., Sloop, C., Pongetti, T., Rao, P., Wong, C., Hopkins, F. M., Yadav, V., Weiss, R. F., Duren, R. M., and Miller, C. E.: Carbon dioxide and methane measurements from the Los Angeles Megacity Carbon Project – Part 1: calibration, urban enhancements, and uncertainty estimates, Atmospheric Chemistry and Physics, 17, 8313–8341, https://doi.org/10.5194/acp-17-8313-2017, 2017.

Welp, L. R., Keeling, R. F., Weiss, R. F., Paplawsky, W., and Heckman, S.: Design and performance of a Nafion dryer for continuous operation at CO_2 and CH_4 air monitoring sites, Atmospheric Measurement Techniques, 6, 1217–1226, https://doi.org/10.5194/amt-6-1217-2013, 2013.